Controllable Preparation of Hydrangea Shaped CoAl-LDHs@CoF2 Composite for Supercapacitor Electrode with Superior Performance

Xue Bai
Fujian University of Technology
Fengyi Sun
Fujian University of Technology
LiYan Ma
Fujian University of Technology
Jyunhong Shen
Fujian University of Technology
Zhuwu Jiang
Fujian University of Technology
Dongdong Xu
Fujian University of Technology
Chuntao Pan
Fujian University of Technology
Hongcheng Di
Fujian University of Technology
Hongyu Zhang (zhyenvironment@126.com)
Fujian University of Technology

Research Article

Keywords:

Posted Date: January 12th, 2024

DOI: https://doi.org/10.21203/rs.3.rs-3847644/v1

Additional Declarations: No competing interests reported.

Controllable Preparation of Hydrangea Shaped CoAl-LDHs@CoF_2 Composite for Supercapacitor Electrode with Superior Performance

Xue Bai[1], Fengyi Sun[1], LiYan Ma, Jyunhong Shen, Zhuwu Jiang*, Dongdong Xu, Chuntao Pan, Hongcheng Di, Hongyu Zhang *

School of Ecological Environment and Urban Construction, Fujian University of Technology, Fuzhou 350000, China

*To whom correspondence should be addressed.
E-mail: jiangzhuwu@126.com; zhyenvironment@126.com

Abstract

Exploring the method for rational design hierarchical structures such as hollow, sphere and core-shell structure is a crucial challenge for enhancing electrochemical performance of supercapacitor electrodes. In this study, we demonstrate a facile method for controllable preparation of hydrangea shaped CoAl-LDHs@CoF_2 composite and used as positive electrode for supercapacitor. A series of contrast tests are performed to select optimal experiment condition. CoAl-LDHs obtained at metal ratio of 2:1, reacting 8 h with addition of NH_4F, displays optimal performance associated with the hierarchical structure, where NH_4F plays a vital role in regulating this uniform generation process. The fabricated working electrode shows high specific capacitance of 827.8 Fg^{-1}, with excellent capacitance retention of 62.8% after current density increases ten times. At last, an asymmetric supercapacitor using C2A1-8h sample as positive electrode and activated carbon as negative electrode, is assembled and delivers an outstanding energy density of 53.7 Wh kg^{-1} at power density of 239.9 kW kg^{-1}, and energy density reaches 27.8 Wh kg^{-1} at maximum power density of 12000 W kg^{-1}, indicating C2A1-8h is a potential candidate for energy storage and conversion systems.

1 Introduction

Considering the increasing environmental pollution caused by fossil fuel combustion，the development of sustainable energy storage system is of great potential such as wind energy, potential energy, electrical energy, nuclear energy[1-4]. While the intermittency of sustainable energy limits their application in a large scale. How to store sustainable energy in safe and green method is still searching for. In this aspect, electrochemical energy storage system such as battery and supercapacitor can resolve this issue[5, 6]. Supercapacitors have been widely studied owing to their superior electrochemical performance such as fast charging and discharging rate, high power output and excellent cycling stability. However, the corresponding utilization is limited by this relatively low specific capacitance, which can only be used as backup energy storage unit in practical application[6, 7].

The essential issue for improving the specific capacitance of electrodes is selecting suitable electrode materials [8, 9]. Depending on the traditional electrochemical energy storage methods, supercapacitors can be divided into two types: electro-chemical double layer capacitors (EDLCs)[10, 11] due to the physical adsorption/desorption, and interfacial fast faradaic reaction. In comparison with EDLCs, the charges are stored by pseudocapacitors based on the redox reaction on the surface of electrodes, endowing the electrode with the characteristics of fast charging/discharging rate, and enhanced energy density[12, 13]. However, the energy density of pseudocapacitor is still relatively low comparing with traditional lithium ion battery under control of electrode materials [14, 15].

Layered double hydroxides (LDHs)[16-18] with the characteristics of high redox efficiency have been widely studied in the field of supercapacitor [19-21]. The special two-dimensional layered structure can offer sufficient electrochemical reaction sites for

redox reactions. Unfortunately, serious agglomeration occurred between LDHs laminates reduce active surface and increase electron transfer resistance[22, 23]. Various methods have been applied to resolve the issue, and mainly divided into three types, (1) Exfoliation of LDHs were prepared into nanosheets, Gunjakar et al. successfully obtained cobalt-chromium hydrotalcite with the layer-by-layer structure of porous self-assembled nanohybrids based on lattice engineering exfoliation-reassembling method, which was intercalated with 0 D polyoxotungstate anions. And this synthesized nanohybrids revealed a high specific capacity of 1303 C g^{-1} with a capacity stability of 85.43 % after 5000 cycles[24]. (2) LDHs hollow architecture via template sacrifice method was constructed. Our previous work fabricated CoMn-LDHs hollow polyhedrons derived from ZIF-67 templates as supercapacitor electrode and exhibiting superior cycling stability with the capacitance retention of 91.2% after 4000 cycles[25]. (3) Controllable construction of LDHs hierarchical structure was regulated. Wu et al. fabricated ZnCo-LDH exhibiting 3D hierarchical microstructure composed of 1D nanoneedles and 2D nanosheets on Ni foam through a simple and effective procedure, which displayed an ultra-high specific capacitance of 3871.2 F g^{-1} at 1 A g^{-1} [26]. Obviously, hierarchical structures are beneficial to optimize the electron transfer path and provide more active sites, which can improve the electrochemical properties of supercapacitor electrodes [27, 28]. Whereas, the approaches during fabrication process are complex and the production is relatively low, which could not meet the demand for practical application[29]. The development of facile method in synthesizing LDHs based materials with hierarchical structure for supercapacitor electrode is still searching for.

In this work, controllable preparation of hydrangea shaped CoAl-LDHs@CoF_2 composites for supercapacitor electrode is developed and used as positive electrode with outstanding properties including high specific capacitance, good rate capability

and superior cycling life. The formation of special hydrangea structure is mainly associated with the metal ions and reacting time along with the addition of NH_4F. The CoAl-LDHs@CoF_2 composite is treated as positive electrode and the activated carbon acted as negative electrode in this asymmetric supercapacitor system, which are assembled for evaluating the potential of practical utilization. High energy density of 53.7 Wh kg^{-1} can be obtained at power density of 239.9 kW kg^{-1}. Moreover, a maximum power density of 12000 W kg^{-1} is obtained and the energy density still remains 27.8 Wh kg^{-1}, manifesting its potential in application in energy storage and conversion system.

2 Experimental Section

2.1 Synthesis of CoAl-LDHs@CoF_2 (CA)

In a typical procedure, 0.29 g NH_4F, 0.50 g $Al(NO_3)_3 \cdot 9H_2O$, 0.78 g $Co(NO_3)_2 \cdot 6H_2O$ and 0.60 g urea were mixed in 70 mL deionized water under stirring condition. The homogeneous solution was transferred to hydrothermal reactor and heated to 120ºC for 3 h, 6 h and 12 h respectively. The precipitate was fully rinsed with DI water and ethanol three times and at last fully dried at 60 ºC overnight. The obtained powders were named as C2A1-4h, C2A1-8h and C2A1-12h, respectively. For comparison, CAL with Co and Al ratios of 1:1 and 3:1 under different reacting time were also prepared

2.2 Characterization and measurement

The scanning electron microscopy (SEM) data were collected on the Sigma 300 of ZEISS from Germany, which was used to analyze the microstructure and morphology of prepared products. The phase and structure information of products were investigated by X-ray diffraction (XRD, Bruker D8 Advance). The surface information of as-prepared samples was recorded on X-ray photoelectron spectrum

(XPS) with the model of Thermo Scientific K-Alpha from USA. BET surface areas with N_2 adsorption/desorption isotherms were tested on Nova instrument (USA, Quantachrome).

The obtained electrodes were achieved through the traditional prepared process including 85% active material, 10% acetylene black and 5% polytetrafluoroethylene, which were stirring in ethanol solvent to construct the uniform slurry. Then, it was coated onto a piece of 1×1 cm^2 carbon cloth. Finally, the electrodes were obtained after fully dried at 70 °C overnight. The electrochemical performance of different samples was tested by a traditional three-electrode system including of saturated calomel electrode (SCE) as reference electrode, Pt foil as counter electrode, and active samples as working electrodes in 1 M KOH aqueous as electrolyte, which employed the CHI660I workstation made in Shanghai of China.

2.3 Asymmetric supercapacitors

An asymmetric system was assembled with activated carbon (AC) as negative electrode, cellulose acetate membrane as separator, and prepared material as positive electrode, respectively. The **Eq. 1** presented the theory of charge balance, which depended on the mass of both electrodes. The **Eq. 2** displayed the mass balance in order to obtain the $q_+=q_-$.

$$q = C \times \Delta V \times m \tag{1}$$

$$\frac{m_+}{m_-} = \frac{C_- \times \Delta V_-}{C_+ \times \Delta V_+} \tag{2}$$

C_+, C_-, were the specific capacitances and $\triangle V_+$, $\triangle V_-$ were the voltage windows of C2A1-8h and AC respectively. The optimum weight ratio between the C2A1-8h and AC was evaluated to be $m_+/m_- \approx 0.51$

The **Eq. 3** revealed the calculated results of specific capacitance of working

electrodes from GCD curves. And the **Eq. 4−5** were used to calculate the power density P (W kg^{-1}) and energy density E (Wh kg^{-1}) for this asymmetric system.

$$Cs=I \times \triangle t/ \triangle V \times m \quad (3)$$

$$E = 0.5 \times Cs \times \Delta V^2 \quad (4)$$

$$P = E \times 3600 / \Delta t \quad (5)$$

3 Results and Discussion

The formation mechanism is displayed in **Fig. 1**. At initial stage, the addition of NH_4F can lead to CoF_2 microsphere. As the time goes on, the CoAl-LDHs nanosheets are gradually formed in-situ on CoF_2, causing the enlarged layered thickness of CoF_2. With the time further prolonging, the collapse of spherical structure occurs, and uniform layered structure is obtained. Above all, NH_4F plays an important role in construction of CA, and the reacting time control the morphology simultaneously.

3.1 Composition identification of CA

In order to explore the formation mechanism of composite materials, the samples at various reaction time states with three proportions of Co/Al are analyzed by X-ray diffraction in Fig. 1. It can be seen that when the ratio of Co/Al is 1:1, the composite materials inherit the phase of CoAl-LDHs with layered structure and CoF_2 with tetragonal form (space group P42/mnm), corresponding to the PDF cards of (JCPDS#54-1030) and (JCPDS#40-0598), respectively. For the XRD patterns of different samples with C1Al-4h, C1Al-8h, and C1Al-12h, the composite maintains the characteristic diffraction peak of hydrotalcite at 2θ=11.6°, 23.3°, 34.6°, 39.1°, 46.7°, related to the lattice planes of (003), (006), (012), (015), (018) from CoAl-LDHs and the peak at 2θ=18.6° belongs to CoF_2, which demonstrates the successful synthesis of composite materials. With the reaction time extended from 4 h to 8 h, the XRD peak density of CoF_2 gradually wanes and the peak at 2θ=11.6°, 23.3°, 34.6° from CoAl-

LDHs gradually enhances. It means that in the composite materials, CoF_2 using $Co(NO_3)_2 \cdot 6H_2O$ and NH_4F sources forms firstly due to the interaction between F ions with strong polarity Co ions, then the CoAl-LDHs material forms based the sources form Co, Al and urea. For further verify this hypothesis, when the ratio of Co/Al is 2:1, the composite shows the obvious main peak at 2θ=18.6° from CoF_2. As the reaction time increases to 8 h, the composite material exhibits the main peak form CoAl-LDHs with layered structure, which demonstrates the formation processes of CoF_2 and CoAl-LDHs. Further improving the ratio of Co/Al to 3:1, the composite reveals the amorphous state without the structures of CoF_2 and LDHs. Meanwhile, without adding NH_4F sources, the only LDHs peaks are observed in Fig. 2b, this result fully proves that F ions with strong polarity are beneficial to the formation of composite materials. Therefore, the composite fully combines the characteristics of CoF_2 as battery material and CoAl-LDHs as capacitor material, which is expected to deliver high energy density and power density.

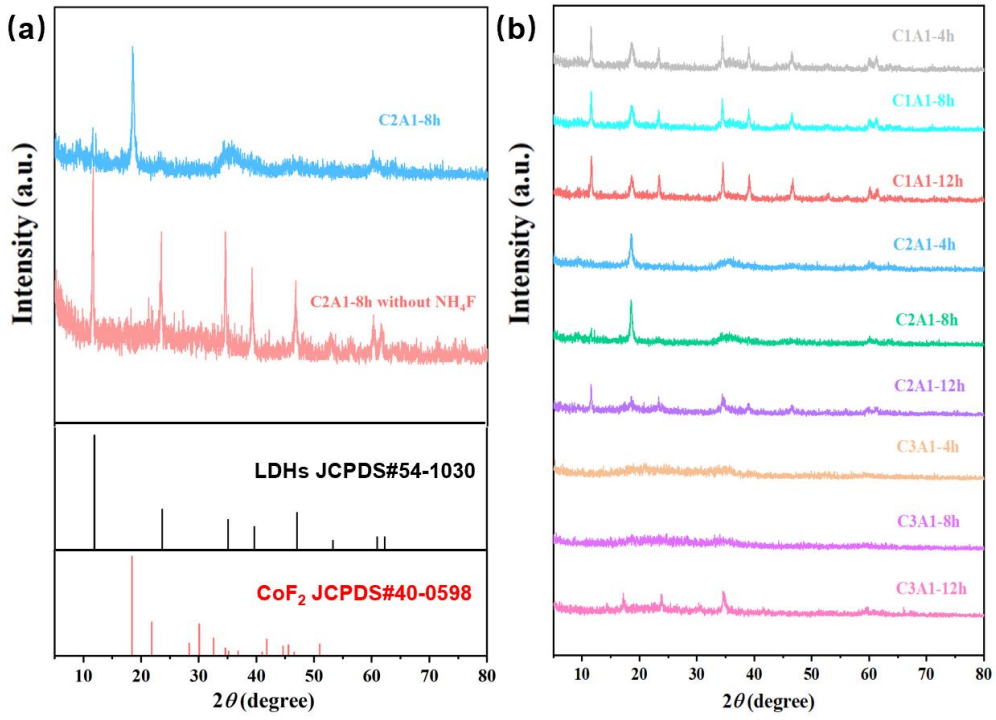

Figure 1. XRD patterns of C2A1-8h with and without addition of NH_4F (a), XRD

patterns of CoAl-LDHs under different reaction conditions including metal ions proportions and reacting time (b).

The composite materials at different states are further manifested by SEM to observe the growth process in Fig. 2. It can be found that when the ratio of Co/Al is 1:1 at 4 h, 8 h, and 12 h, the morphology of composite shows agglomerate sheets including CoF_2 and CoAl-LDHs, of which the size is ~12 μm at initial stage (Fig. 2a). As the reaction time increases to 8h, the morphology of composite changes to hydrangea-like structure with the smaller size, which is constructed by CoF_2 as hydrangea skeleton and CoAl-LDHs grows along this skeleton. However, the morphology of composite still shows agglomerate phenomenon and CoAl-LDHs sheets are not obvious (Fig. 2b). At the state of 12 h, the hydrangea-like structure of composite materials collapses and the mixing sheets change thicker. These results are in good line with the XRD patterns. And the hypothesis on the growth process of composite materials is further proved in Fig. 2d-f. It can be clearly found that when the ratio of Co/Al is 2:1, during the initial 4 h, the hydrangea-like skeleton of CoF_2 is generated first, then CoAl-LDHs sheets grow between the CoF_2 flower sheets at 8h, which is consistent with the XRD results of C2A1-8h sample (Fig.1). After 12h, the structure of composite also collapses. When the ratio of Co/Al is 3:1 at 4 h, 8 h, and 12 h, the morphology of composite shows ball-like or irregular agglomeration sheets in Fig. 2g-2i. Meanwhile, the morphology of CoAl-LDHs without NH_4F samples is also shown in Fig.S1 for comparison. Therefore, the sample of C2A1-8h for composite material exhibits the optimum hydrangea-like morphology, which inherits the potential to exhibit excellent electrochemical properties.

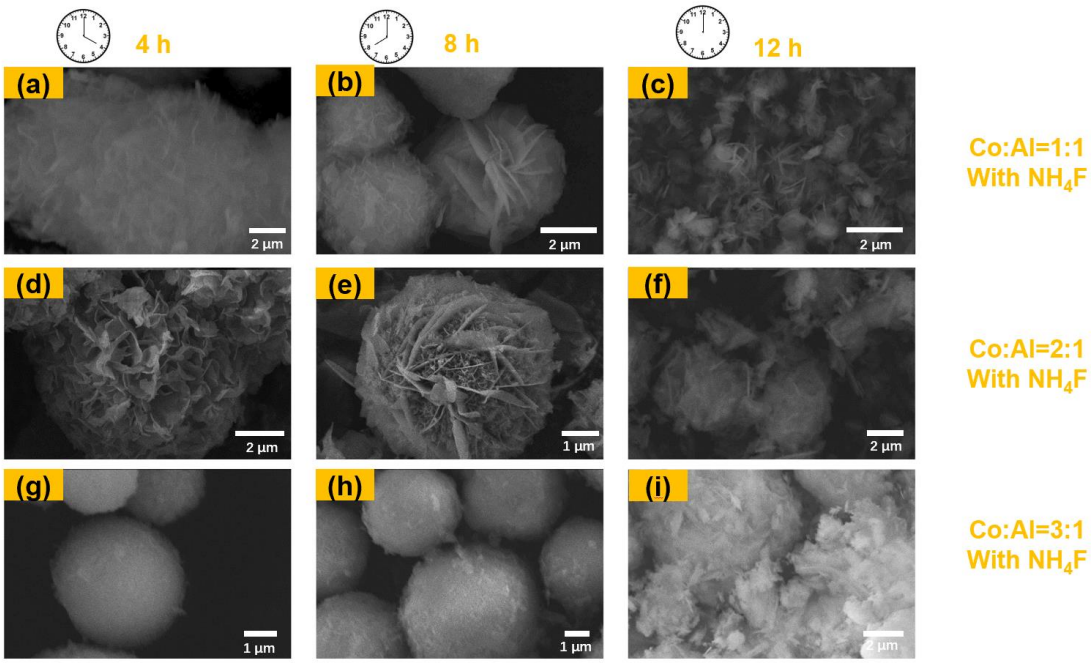

Figure 2. SEM images of CoAl-LDHs under different reaction conditions including metal ions proportions and reacting time, Co:Al=1:1 with under reacting time of 4h (a), 8 h (b) and 12 h (c). Co:Al=2:1 with under reacting time of 4h (d), 8 h (e) and 12 h (f). Co:Al=3:1 with under reacting time of 4 h (g), 8 h (h) and 12 h (i).

Further to explore architectural feature of composite materials with C2A1-8h sample, TEM and XPS are performed as displayed in Fig. 3. It can be found that CoF_2 sheets are tightly integrated with CoAl-LDHs sheets. Fig. 3b shows the high magnification image of composite material and the black parts are the CoF_2 skeletons, and the gray parts are the CoAl-LDHs thin sheets, which prove that the composite material are prepared successfully. The XPS measurement is carried out to determine the oxidation states of different elements on the surface of composite materials. Fig. 3c displays the full-scale XPS spectra of C2A1-8h, which is composed of F, Co, Al, O and C on the surface. Fig. 3d shows that the Co 2p spectrum has two peaks located at 782.4 eV and 798.4 eV, corresponding to the spin-orbital splitting of Co $2p_{1/2}$ and $2p_{3/2}$, which can be attributed to the Co^{2+30}. Fig. 3d shows that the Al 2p spectrum owns single peak at 74.8 eV, which is assigned to the characteristic peak of Al $2p_{1/2}$ and it can be attributed

to the Al^{3+}[31]. These results indicate that the prepared CoAl-LDHs@CoF_2 composite inherits their own stable valence state and play more excellent electrochemical performance.

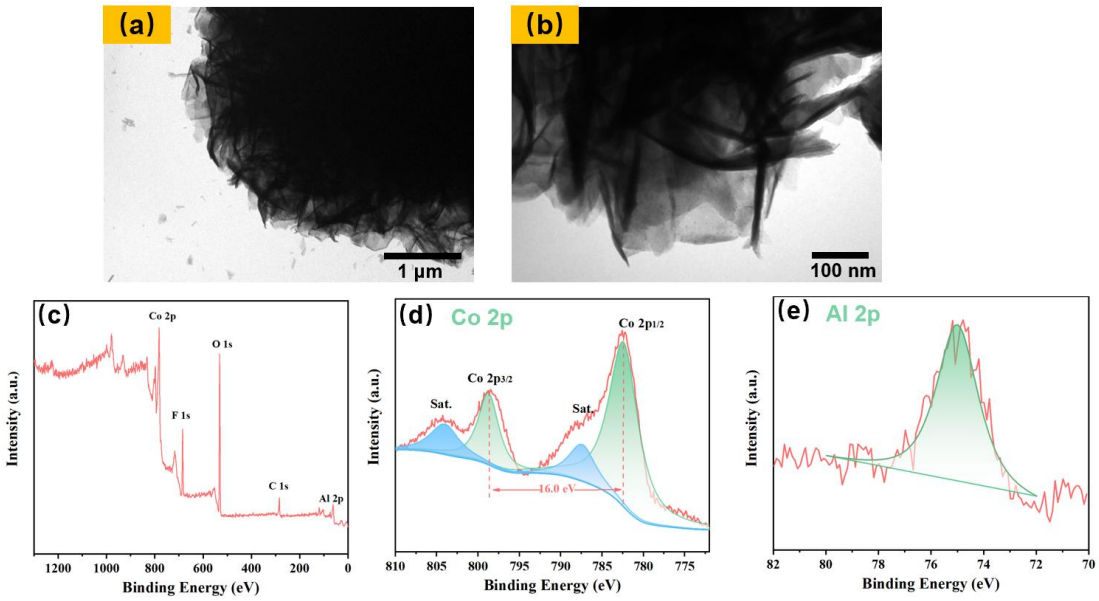

Figure 3. TEM images of C2A1-8h sample (a-b), XPS spectra of survey scan (c), and high-resolution spectra in the regions of Co 2p (d) and Al 2p (e).

The electrochemical behaviors of composite materials are evaluated in the traditional three-electrode system by employing the Pt plate as counter electrode, calomel electrode as reference electrode, active material as working electrode in 1 M KOH as electrolyte. Fig. 4a shows the cyclic voltammograms (CV) curves of CoAl-LDHs with different metal ratios under various reacting periods. The voltage range of samples are performed between 0 V and 0.65V vs.SCE at the constant scan rate of 5 mV s^{-1}. It can be clearly found that nine CV curves all present one pair of redox peaks accounted for the changes in the valence of cobalt for composite materials, which shows the faradaic reaction (**Eq**. 6-8). Moreover, the C2A1-8h sample with the CoAl-LDHs shell anchored to a skeleton of CoF_2 exhibits a larger enclosed CV area and higher current density due to the unique morphology and structure delivered faster ion

transport path, which indicates a high specific capacitance of this sample. The conjecture is further confirmed by charge-discharge curves as displayed in Fig. 4b at current density of 1 A g^{-1}. The specific capacitance of C1A1-4h, C1A1-8h, C1A1-12h, C2A1-4h, C2A1-8h, C2A1-12h, C3A1-4h, C3A1-8h and C3A1-12h are 526.3 Fg^{-1}, 179.9 Fg^{-1}, 149.8 Fg^{-1}, 560.2 Fg^{-1}, 827.8 Fg^{-1}, 599.2 Fg^{-1}, 277.6 Fg^{-1}, 513.6 Fg^{-1} and 199.2 Fg^{-1}, respectively. A maximum specific capacitance of 827.8 Fg^{-1} is obtained for C2A1-8h sample, which is much higher than other samples and the result is consistent with CV curves. The high specific capacitance may be associated with the low resistance of electrodes.

$$Co(OH)_2 + OH^- \leftrightarrow CoOOH + H_2O + e^- \quad (6)$$

$$CoOOH + OH^- \leftrightarrow CoO_2 + H_2O + e^- \quad (7)$$

$$CoF_2 + OH^- \leftrightarrow CoF_2OH + H_2O + e^- \quad (8)$$

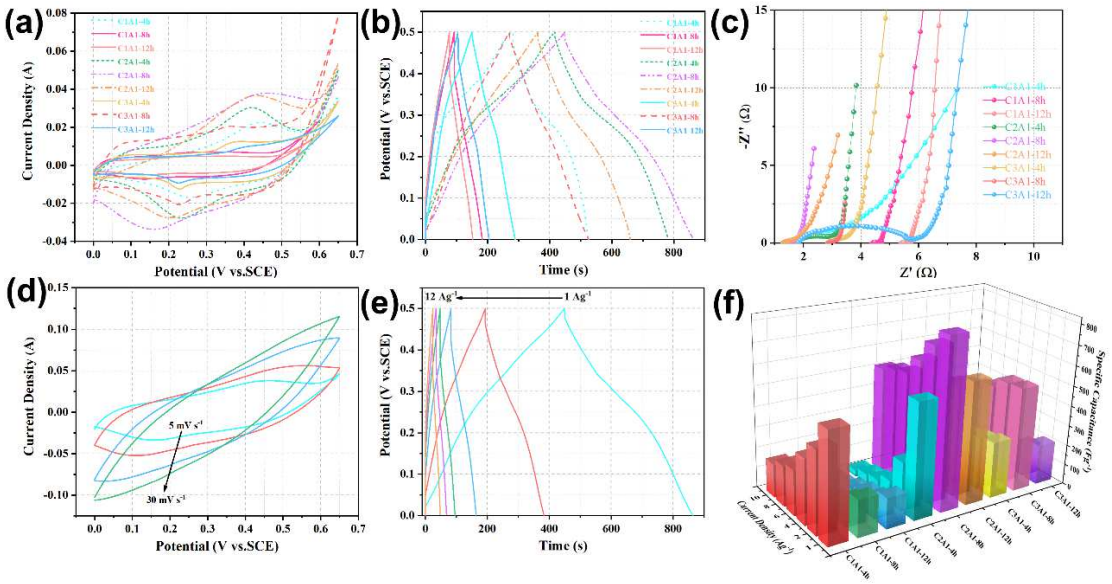

Figure 4. CV curves (a), GCD curves (b) and EIS results (c) of CoAl-LDHs under different reaction conditions including metal ions proportions and reacting time, CV curves of C2A1-8h sample at various scan rates (d), GCD curves of C2A1-8h sample obtained at different current densities (e) and comparison of the capacity of nine

samples.

In order to certify the conclusion, EIS tests are used to check the ability to transfer electrons in Fig. 4c. All nine curves are composed of a semicircle in high frequency and a straight line in low frequency, corresponding to the charge transfer resistance (Rct) and the ion diffusion between the surface of electrode and the electrolyte. Notably, the C2A1-8h electrode shows the smallest Rs and Rct values in all samples, which is beneficial to diffuse rapidly for electrons. Above all, C2A1-8h exhibits excellent electrochemical performance. The high performance is associated with the hierarchical hydrangea structure, where the ultrathin CoF_2 nanosheets are beneficial for contacting with electrolyte and the interfacial formation of CoAl-LDHs provides fast electron transfer skeleton. The appropriate thickness of layers provide assurance for providing active area and the hydrangea structure can accommodate the expansion and contraction during long-term charging and discharging processes.

Fig. 4d shows CV curves of C2A1-8h recorded at various sweep rates ranging from 5 mV s^{-1} to 30 mV s^{-1}. Obvious redox peaks can be identified at all scan rates, indicating the contribution of redox reaction. As the scan rate increases, the redox peaks shift to more positive and negative directions. The CV curve doesn't display obvious distortion although at high scan rate of 30 mV s^{-1}, suggesting the superior rate capability of C2A1-8h. Based on the plots of GCD curves, the maximum specific capacitance of C2A1-8h is calculated to be 827.8 F g^{-1} at current density of 1 A g^{-1}, the specific capacitance can still remain 520.2 F g^{-1} though the current density increases ten times, displaying about 62.8% capacitance retention. Fig. 4f summarizes the capacitance of CoAl-LDHs prepared at different metal ratios under different reacting time to further compare the rate capability of nine samples. Significantly, after current density increases ten times, the rate retentions of C1A1-4h, C1A1-8h, C1A1-12h,

C2A1-4h, C2A1-8h, C2A1-12h, C3A1-4h, C3A1-8h and C3A1-12h are 31.2%, 14.3%, 13.4%, 5.4%, 62.8%, 56.2%, 66.1%, 73.7% and 14.4%, respectively. To sum up, C2A1-8h sample is selected as optimal electrode material for further test.

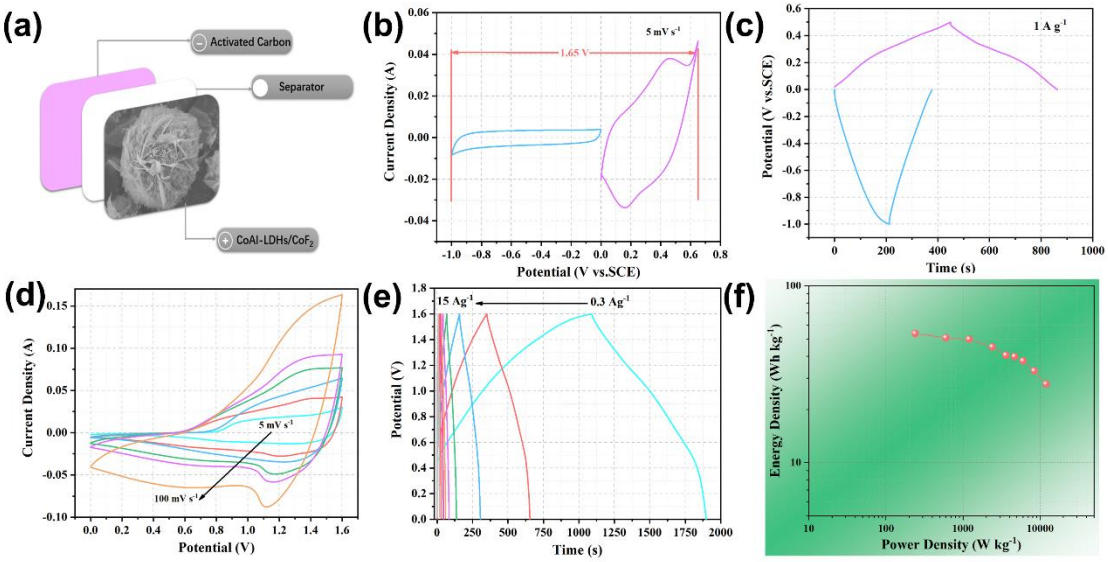

Figure 5. Schematic illustration of the assembled C2A1-8h//AC device (a), CV (b) and GCD (c) curves of C2A1-8h and activated carbon, CV curves of assembled supercapacitor at various scan rates from 5 mV s^{-1} to 100 mV s^{-1}, GCD curves of device at different current densities (e) and Ragone plot of assembled device.

To investigate the utilization potential of prepared materials, an asymmetric supercapacitor is assembled with activated carbon as negative electrode and C2A1-8h as positive electrode with a separator between two electrodes, as illustrated in Fig. 5a. Before assembly, the CV curves of activated carbon and C2A1-8h are tested to certify the working potential range. Activated carbon displays stable potential range from -1 to 0 V vs.SCE, and that for C2A1-8h is 0 to 0.65 V vs.SCE. However, polarization phenomenon occurs as the potential increase up to 0.6 V vs.SCE, thus 1.6 V is selected as working potential range for the assembled supercapacitor to protect the electrode. The charge-discharge curves of C2A1-8h and activated carbon is further certify the optimal voltage window. Fig. 5d exhibits CV curves of assembled device at different

scan rate from 5 mV s^{-1} to 100 mV s^{-1}. Pseudo rectangle involving redox peaks can be observed during the potential window, indicating the contribution of capacitance involves double layer capacitance and pseudocapacitance. The redox peaks shift along with the increase of scan rate. Although at high scan rate, no significant change occurs for CV curve, indicating excellent rate capability of assembled supercapacitor. Fig. 5e displays charge-discharge curves of assembled device tested at different current densities from 0.3 A g^{-1} to 15 A g^{-1}. The maximum specific capacitance of 151.1 F g^{-1} is obtained for assembled device at current density of 0.3 A g^{-1}. A high capacitance of 78.3 F g^{-1} still remains although current density increases 50 times, certifying superior rate performance of assembled supercapacitor. Based on GCD curves, energy and power densities can also be calculated via **Eq. 4-5** and plotted in Ragone plot, as shown in Fig. 5f. The C2A1-8h//AC device delivers the maximum energy density of 53.7 Wh kg^{-1} at power density of 239.9 kW kg^{-1}, and energy density reaches 27.8 Wh kg^{-1} at maximum power density of 12000 W kg^{-1}, again indicating its potential for practical application. Moreover, after repeating charge-discharge curves 5000 times, the capacitance retention still remains 95%, indicating good stability of asymmetric supercapacitor. The assembled device can also drive two LED lights, further proving the practical potential of device in energy storage and conversion system.

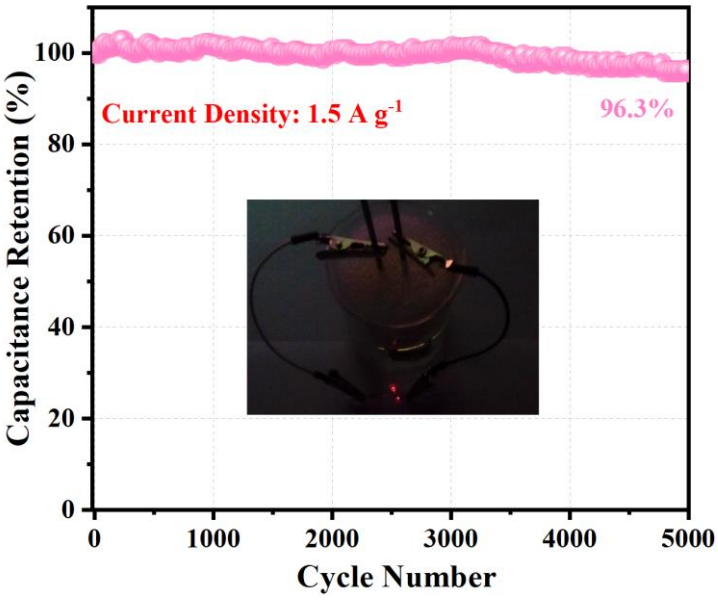

Figure 6. Cycling stability of assembled supercapacitor at current density of 1.5 A g^{-1}, the inset displays the photograph of assembled device driving two LED lights.

Conclusion

In our work, the composite material of CoAl-LDHs@CoF_2 with hierarchical structure is successfully prepared and the optimal sample of C2A1-8h electrode with unique morphology and excellent electrochemical performance is explored. In the three-electrode system, the CV curve of C2A1-8h electrode displays one pair of redox peaks accounted for the changes in the valence of cobalt for composite materials, which shows the obvious faradaic reaction. At the current density of 1 A g^{-1}, the specific capacitance of C2A1-8h is 827.8 Fg^{-1}, which is much higher than other sample electrodes. Meanwhile, the asymmetric supercapacitor is assembled with activated carbon as negative electrode and C2A1-8h as positive electrode, which reveals the maximum energy density of 53.7 Wh kg^{-1} at power of 239.9 kW kg^{-1}, and energy density reaches 27.8 Wh kg^{-1} at maximum power density of 12000 W kg^{-1}. At the current density of 1.5 A g^{-1}, this device exhibits excellent cyclic stability with the capacity retention ratio of 95% after 5000 cycles. This C2A1-8h sample owned the

CoAl-LDHs shell anchored to a skeleton of CoF_2 contributes to the faster ion transport path, which exhibits higher energy density and power density.

Declarations

Conflict of interest The authors declare that they have no conflict of interest.

Ethical approval Not applicable.

Funding This work is supported by the National Natural Science Foundation of China (No.52070043); Natural Science Foundation of Fujian Province (2021J011053); Natural Science Project of Fujian Provincial Department of Finance (GY-Z23015); Fujian Province Science and Technology Department project (GY-Z23067).

Availability of data and materials Not applicable.

References

1. L. Zhang, B. Zhang, X. W. Dou and W. Yan, *Frontiers in Energy*, 2023.
2. S. Lee, J. Hong and K. Kang, *Advanced Energy Materials*.
3. B. Llamas, M. F. Ortega, G. Barthelemy, I. D. Godos and F. G. Acién, *Energy Conversion and Management*, 2020, **210**, 112695.
4. H. Pachori, P. Baredar, T. Sheorey, B. Gupta, V. Verma, K. Hanamura and T. Choudhary, *Journal of Energy Storage*, 2023.
5. M. B. S. M. Wabaidur, S. M. Wabaidur, C. o. S. Saikh Mohammad Wabaidur Saikh Mohammad WabaidurChemistry Department, King Saud University, Riyadh , Saudi ArabiaMore by Saikh Mohammad Wabaidur, a. , M. B. S. Aftab, S. Aftab, S. U. Sikandar Aftab Sikandar AftabDepartment of Intelligent Mechatronics Engineering, Neungdong-ro, Seoul , Gwangjin-gu, South KoreaMore by Sikandar Aftab, M. B. S. Siddique and S. Siddique, *Energy And Fuels*, 2023, **37**, 4000-4009.
6. M. Z. Iqbal, M. W. Khan, M. Shaheen, S. Siddique, S. Aftab, M. Alzaid and M. J. Iqbal, *Journal of Energy Storage*, 2022.
7. S. Biswas and A. Chowdhury, *Chemphyschem: A European journal of chemical physics and physical chemistry*, 2023.
8. B. Bai, L. Qiu, Y. Wang, X. Jiang, J. Shui, Y. Yuan, L. Song, J. Xiong and P. Du, 2022.
9. A. Majdi, A. K. Wadday and Z. S. Abbas, *Inorganic Chemistry Communications*, 2023.
10. D. Kumar, N. Yadav, K. Mishra, R. Shahid, T. Arif and D. K. Kanchan, *Journal of Energy Storage*, 2022, 46.
11. S. Konwar, D. Singh, K. Strzakowski, M. N. Masri, M. Yahya, M. Diantoro, S. Savilov and P. Singh, *Molecules*, 2023, **28**.
12. G. Jialin, L. Wenjing and Z. Peng, *Applied physics, A. Materials science & processing*, 2023.
13. C. Chen, M. Liu, Z. Liu, M. Xie, L. Wan, J. Chen, Y. Zhang, C. Du and D. Li, *Journal of Colloid and Interface Science*, 2022, **614**, 66-74.
14. M. Khot and A. Kiani, *International journal of energy research*, 2022.
15. T. F. Y. A. D. E, H. M. K. S. B, X. L. A. D, F. W. A. D, Y. R. Z. D, J. H. F, J. Z. B. C and X. L. B, *Nano Energy*, 2021.
16. J. Wang, N. Wen, Y. Wang, X. Jiao, D. Chen and Y. Xia, *Applied Surface Science: A Journal Devoted to the Properties of Interfaces in Relation to the Synthesis and Behaviour of Materials*, 2023.
17. D. Wu, X. Hu, Z. Yang, T. Yang, J. Wen, G. Lu, Q. Zhao, Z. Li, X. Jiang and C. Xu, *Industrial & Engineering Chemistry Research*, 2022, 61.
18. B. Zhang, J. Li, Q. Song and H. Liu, *International journal of energy research*, 2022, 46.
19. X. Cao, M. Yuan and C. Ding, *New Journal of Chemistry*, 2023.
20. M. Kour, S. Verma, P. Mahajan, B. Padha, A. Singh, A. Ahmed, A. K. Sundramoorthy and S. Arya, *Materials Science & Engineering, B. Solid-State Materials*

for Advanced Technology, 2023.
21. P. K. Ray, R. Mohanty and K. Parida, *Journal of Energy Storage*, 2023.
22. X. Ju, Z. Yang, D. Wang, X. Duan, Y. Xin, H. Zhu, X. Li, Y. Li, D. Yao and Y. Zheng, *Chemical Engineering Journal*, 2023, **455**, 140797-.
23. P. Wang, S. Song and M. He, *Chem Catalysis*, 2023.
24. S. V. Sadavar, N. S. Padalkar, R. B. Shinde, A. S. Patil, U. M. Patil, V. V. Magdum, Y. M. Chitare, S. P. Kulkarni, S. B. Kale, R. N. Bulakhe, D. S. Bhange, S. T. Kochuveedu and J. L. Gunjakar, *Energy Storage Materials*, 2022, **48**, 101-113.
25. H. Zhang, H. Di, D. Cao, Z. Jiang, Z. Hu and X. Bai, *International Journal of Energy Research*, 2022, **46**, 19599-19614.
26. C. Wang, W. Wu, C. Zhao, T. Liu, L. Wang and J. Zhu, *Journal of Colloid and Interface Science*, 2021, **602**, 177-186.
27. Y. Zhu, QuanZhang, QilongYang, HuiDu, WeiWang, QianqianZhan, JianhuiWang, Huiying, *Electrochimica Acta*, 2020, **334**.
28. W. Cao, C. Xiong, Y. Liu, F. Xu, W. Zhao, Q. Xia, G. Du and N. Chen, *Journal of Alloys and Compounds: An Interdisciplinary Journal of Materials Science and Solid-state Chemistry and Physics*, 2022, 902.
29. J. Yuan, Y. Li, G. Lu, Z. Gao, F. Wei, J. Qi, Y. Sui, Q. Yan and S. Wang, *ACS applied materials & interfaces*, 2023.
30. X. Bai, Q. Liu, J. Liu, Z. Gao, H. Zhang, R. Chen, Z. Li, R. Li, P. Liu and J. Wang, *Chemical Engineering Journal*, 2017, **328**, 873-883.
31. Y. Wang, X. Dai, Q. Zhou, K. Li, L. Feng, W. Liao, Y. Yu, H. Yu, X. Zong, G. Lu and Y. Zhang, *Colloids and Surfaces A: Physicochemical and Engineering Aspects*, 2022, **636**, 128139.

Supplementary Files

This is a list of supplementary files associated with this preprint. Click to download.

- SupportingInformation.doc